Engineering Research Express

INCLUSIVE PUBLISHING TRUSTED SCIENCE

PURPOSE-LED PUBLISHING™

PAPER • **OPEN ACCESS**

UWB distance estimation errors in (non-)line of sight situations within the context of 3D analysis of human movement

To cite this article: Vinish Yogesh *et al* 2024 *Eng. Res. Express* **6** 045303

View the article online for updates and enhancements.

You may also like

- An improved positioning method based on compensation and optimization of ultra-wideband ranging results
Zhiran Shi, Jie Wang, Xianyang Zeng et al.
- An enhanced mobile localization algorithm integrating multiple AUKF models for mixed indoor environments
Yi Jiang, Heng Gao, Pengpeng Zhang et al.
- A Hopular based weighting scheme for improving kinematic GNSS positioning in deep urban canyon
Zelin Zhou, Baoyu Liu and Hongzhou Yang

This content was downloaded from IP address 130.89.47.44 on 27/11/2024 at 11:12

Engineering Research Express

PAPER

UWB distance estimation errors in (non-)line of sight situations within the context of 3D analysis of human movement

Vinish Yogesh[1,2], **Jan Willem A Rook**[1,2], **Thomas Keizers**[1,2], **Carsten Voort**[3], **Jaap H Buurke**[1,2], **Peter H Veltink**[2] **and Chris T M Baten**[1,2]

[1] Roessingh Research and Development, Roessinghsbleekweg 33B, 7522 AH Enschede, The Netherlands
[2] Department of Biomedical Signals and System, University of Twente, Drienerlolaan 5, 7522 NB Enschede, The Netherlands
[3] Gable Systems, Granaatstraat 21, 7554 TN Hengelo, The Netherlands

E-mail: v.yogesh@rrd.nl **and** v.yogesh@utwente.nl

Keywords: ultra-wideband, human body non-line of sight, distance estimation, distance error, 3D analysis of human movement, UWB error characterization

OPEN ACCESS

RECEIVED
5 June 2024

REVISED
23 August 2024

ACCEPTED FOR PUBLICATION
23 September 2024

PUBLISHED
3 October 2024

Original content from this work may be used under the terms of the Creative Commons Attribution 4.0 licence.

Any further distribution of this work must maintain attribution to the author(s) and the title of the work, journal citation and DOI.

Abstract

Integrated Ultrawideband (UWB) and Magnetic Inertial Measurement Unit (MIMU) sensors are becoming popular for indoor localization applications, as a higher accuracy can be achieved than with just MIMU sensors. These integrated sensors could extend stability and accuracy in the field of 3D analysis of human movement (3D AHM) if they can deliver position estimates with an accuracy close to 1 cm. Achieving this high accuracy of 1 cm remains challenging, with most studies reporting position estimation errors around 5 cm, often due to Non-Line of Sight (NLOS) conditions and systematic UWB sensor distance estimation errors. Studying the distance error characteristic of UWB in situations of 3D AHM is essential to deal with these errors. While research on UWB distance errors in Line of Sight (LOS) and NLOS situations exists, few studies focus on the NLOS errors caused by the human body and were not in the relevant scenarios of 3D AHM. Therefore, this article examines UWB sensor performance and distance error characteristics in LOS and NLOS situations typical for the 3D AHM. Both the LOS and NLOS situations were studied in the typical 3D AHM distance range of 0.2 m to 2 m. The NLOS situations were studied first with a human subject as NLOS causing object and then with simulated human body segments (PVC pipes filled with water) of varying diameters. In LOS situations, consistent systematic bias errors were observed, along with incidental errors at specific positions in the room. In NLOS scenarios caused by the human and simulated body segments, a consistent and reproducible overestimation of distances was found. The reproducibility of these errors based on relative node and object positions suggests that systematic mitigation methods could significantly reduce errors, enabling more accurate and reproducible 3D human movement analysis.

1. Introduction

Integrated Ultrawideband (UWB) and Magnetic Inertial Measurement Unit (MIMU) sensors have become popular in estimation of accurate positions for localization and pedestrian navigation applications. This is mainly due to their complementary error characteristics, which can be exploited in data fusion approaches to achieve better accuracy than from the use of these sensors independently [1, 2]. Specifically, kinematics estimation algorithms driven by MIMU sensor data are affected by integration drift errors [3, 4] for both position and orientation estimates, but are not affected by Non-Line of Sight (NLOS) situations. While the UWB sensors are capable of delivering drift-free position estimates driven by absolute distance measurements, they are strongly affected by NLOS situations [2, 5]. The UWB technology stabilizes the integration drift in position estimation, which typically occurs in solutions using only MIMUs, by offering directly measured distance or (relative) position updates to a data fusion-based estimator. Additionally,

© 2024 IOP Publishing Ltd. All rights, including for text and data mining, AI training, and similar technologies, are reserved.

UWB technology is a cost-effective solution that operates across a wide frequency spectrum (3.1 GHz to 10.6 GHz) and offers significantly higher accuracy in indoor positioning compared to other wireless systems like Bluetooth, LiDAR, and GPS [6, 7]. To achieve good UWB/MIMU data fusion results, the UWB distance estimates have to possess very low or no systematic errors. Therefore, the accuracy with which the UWB system can deliver these updates is very relevant to the accuracy that can be achieved by the data fusion-based position estimator.

The integrated UWB/MIMU sensor systems could bring a great improvement to the ambulatory 3D analysis of human movement (3D AHM) if they can achieve accuracies in position estimation similar to the vision-based measurement systems such as Vicon [6]. This is attributed to the fact that the vision-based measurement system is considered to be the 'gold standard' and is deemed clinically relevant for 3D AHM, with position estimation errors less than 1 cm [8, 9]. Therefore, a systematic error of 1 cm or less in position estimation is targeted. However, the smallest errors in position estimation reported so far by these integrated UWB/MIMU sensor systems are around 4 cm [10, 11], which is not sufficient for the 3D AHM application. Also, these were achieved in most ideal conditions i.e. in clear Line of Sight (LOS) situations [6]. For the NLOS situation (a typical 3D AHM situation), almost all studies on the integrated UWB/MIMU sensors reported position estimate errors greater than 10 cm [6, 12, 13]. Most of these studies indicate that the high errors in the UWB distance estimates, as the main cause for this position estimate errors in UWB/MIMU data fusion [6]. This again suggests that improvement of the UWB distance estimates could potentially improve the accuracy of position estimation through UWB/MIMU data fusion to accuracies required in 3D AHM applications.

UWB systems are reported to deliver distance estimates with sub-centimeter-level accuracy in ideal controlled environments such as an anechoic chamber [7, 14]. However, in real-life applications, this high accuracy can only be achieved in LOS situations, like in unobstructed free (outdoor) space [15]. In indoor environments, the accuracy of UWB typically tends to drop significantly, because of the presence of complex varying obstacles such as furniture, human bodies, and building infrastructure (walls, floors, furniture, and pillars) that disturb the UWB ranging accuracy by causing NLOS situations and additional disturbances by reflections [16]. For application in 3D AHM, multiple UWB nodes would be mounted on the human skin or body surface, which would perform distance-ranging measurements between each other and sometimes also with external sensor nodes. In this application, NLOS situations caused by human body segments will occur regularly [7]. As a result, overestimation of distances would occur to an extent that suggests that the distance of the shortest pathway around the obstruction is measured [17].

There are multiple research on the mitigation of errors occurring due to NLOS situations and are all described in these comprehensive review articles [18, 19]. However, only a limited number of research among them are aimed towards mitigating the effects of NLOS caused by human body [7, 20–26], a typical NLOS situation of 3D AHM application. The lowest position estimation errors after utilizing these mitigation strategies were reported to be around 12 cm [22], with all other methods higher than 20 cm and these are still not suitable for the application of 3D AHM. A comprehensive study of UWB distance estimation error characteristics and behaviour in scenarios specific to 3D AHM is crucial for advancing research on developing targeted mitigation strategies tailored to this application.

The typical 3D AHM application scenario consists of distance measurements between on-body UWB sensor nodes and possibly a few external UWB nodes, all within the distance range of 0.2 m to 1.8 m. Besides, all the NLOS-induced errors are caused by human body segments being present either in between on-body nodes or between an on-body and external node. The UWB distance or ranging error characteristics found in the literature are mostly reported for LOS situations and NLOS situations caused by infrastructures in the measurement environment [19]. There are no studies on LOS situations within short distance ranges relevant to 3D AHM scenarios and only a few studies report on NLOS effects caused by human body segments [15, 22, 26–29]. All these reported studies on NLOS effects caused by human body, examined situations with the inter-node distances being 1 m or (much) larger, while typical 3D AHM situations would have distances around 1.5 m and smaller. Also, all of these reports only considered scenarios with a human subject present in between two ranging nodes at some distance, while this was not studied for two or more on-body sensors. The study by Jie *et al* [15] and Tian *et al* [22], were the only reported NLOS experiments among the identified literature, that measured the distance between a single on-body sensor node and one fixed anchor node at some distance.

To the best of the authors' knowledge, there are no studies that study the errors of UWB in short ranges relevant for 3D AHM scenarios in both the LOS and for NLOS due to human interference, as well as no studies on errors in distance between on-body sensors. Also, there is very limited research and information on the behavior of UWB sensors in NLOS situations caused by the human body. Therefore, this article aims to study the

UWB distance estimation performance and error characteristics under conditions typically occurring in the 3D AHM application, with the purpose of identifying the possibilities to maximize future mitigation of these errors in the intended application. The novelty introduced by this article lies in the examination of specific conditions for 3D AHM that have not been previously explored:

1. Distance errors in LOS situations for short ranges (0.2 m and 1.8 m) relevant to 3D AHM.
2. Distance errors in NLOS situations caused by the human body, both when both UWB sensors are on the body and when one sensor is on the body with the other off the body.
3. Distance errors in NLOS situations caused by varying thicknesses of the human body, achieved using simulated human body segments of different diameters, all within the distance ranges relevant to 3D AHM.

The remainder of the article is organized as follows: section 2 outlines the detailed methodology for error characterization, including a description of the UWB measurement system used in this study and the experimental setup. Further, describes the experimental scenarios designed for error characterization. Section 3 presents the observed error characteristics across the various tested scenarios. Finally, section 4 offers an in-depth discussion of the observed error characteristics and analyzes their implications for the intended application of 3D AHM.

2. Methods

2.1. UWB measurement system

The UWB sensors or measurement system used in this research was a customized fully integrated UWB/MIMU sensor hardware platform developed in-house, named 'UMIMU' sensor system (Ultra-wideband Magnetic Inertial Measurement Unit sensor system; figure 1(a)). The UMIMU sensors included a UWB transceiver module DWM1000 (Qorvo Inc., Greensboro, USA) combined with a 9-axis MTi-3 MIMU (Xsens Technologies, Enschede, Netherlands). The DWM1000 UWB module used in this paper was operated in channel 2 with a center frequency of 3.9 GHz (bandwidth of 3.7 GHz to 4.2 GHz), utilizes Binary Phase Modulation (BPM) combined with Binary Phase Shift Keying (BPSK) for signal modulation and supports a theoretical range of up to 300 m. An STM32F722R microcontroller (STMicroelectronics, Geneva, Switzerland) controlled the node configurations, the node role attribution and the effective swarm topology and ranging in a round-robin scheme optimized for minimal (and known) time between individual ranging actions between node pairs within each update. Additionally, it also controlled the data transport of UWB distance measures as well as the full 3D MIMU kinematics data from UMIMU nodes to the PC. The UMIMU was also equipped with a USB port for charging, configuration, and data communication.

This paper examines the performance of the UWB sensors in the UMIMU modules under (N)LOS situations. Therefore, for reasons of readability, in the rest of the paper we refer to the UWB sensors in the UMIMU modules simply as 'UWB nodes'. The UWB nodes estimate the distance between two ranging nodes by the Alternative Double-Sided-Two Way Ranging (AltDS-TWR) method as described in Neirynck *et al* 2016 [30]. Also, all the UWB nodes used in this study were (re-)calibrated for the antenna delay settings to minimize ranging errors as per the manufacturer's manual [31]. The UWB data were recorded at an update rate of 27.73 or 36 samples per second for a set of 3 or 2 ranging UWB nodes in the network, respectively. The data of the MIMU sensors in the UMIMUs was recorded but was only used to synchronize the UWB ranging data with data of the vision-based reference system. The MIMUs delivered 100 samples per second comprising 3D orientation, acceleration, and angular velocity.

The UMIMU sensors were specifically developed for the intended use in a typical 3D AHM application with only on-body UMIMUs in a swarm topology. In this topology, ranging operations are performed between all possible UWB node pairs in the swarm. The physical configuration of the UWB sensor system comprises three or more nodes (which are all physically the same) of which one node assumes the role of 'controller node' and the remaining nodes assume roles of ranging initiator or ranging responder (figure 1(b)). The controller node always remains connected to a PC via a USB connection and is used to configure and control the node roles, ranging operation, and collecting all the distance estimates between the ranging UWB nodes for the PC. Also, the MIMU data is transported from all ranging nodes through the controller node to the PC, where it is stored along with the ranging data for further processing (in this case only for synchronization purposes).

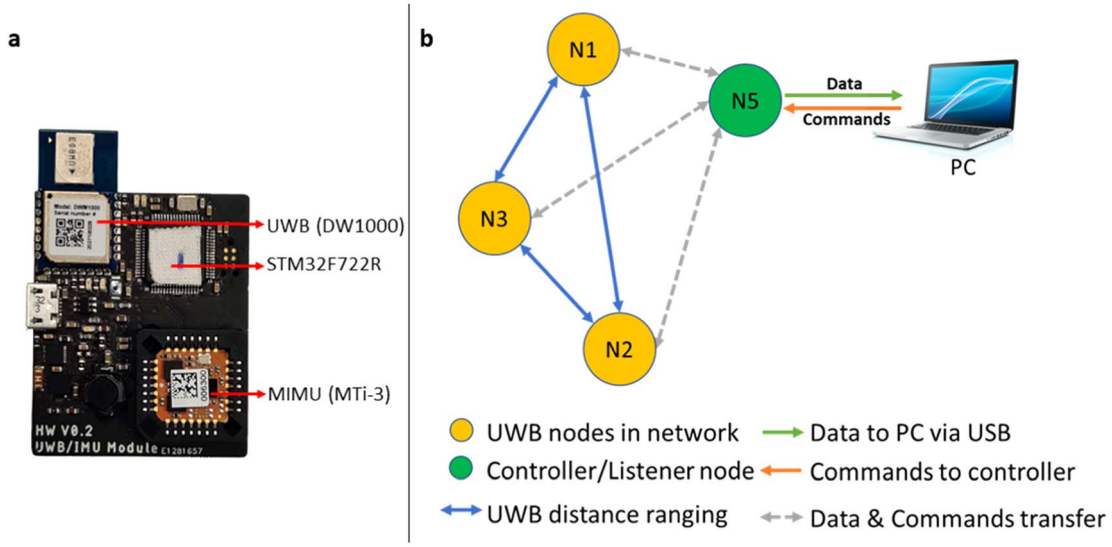

Figure 1. (a) UMIMU sensor hardware; (b) Typical UMIMU sensor system configuration with swarm topology and their functioning.

2.2. Distance estimation error definition

The true distance between two ranging UWB nodes (sensor i and j) is defined as $D_{true\ i,j}$ and the estimated distance between the ranging UWB nodes is defined as $D_{uwb\ i,j}$. The distance estimation error $D_{error\ i,j}$ is defined as the difference between the estimated distance and the true distance:

$$D_{error\ i,j} = D_{uwb\ i,j} - D_{true\ i,j} \tag{1}$$

2.3. Error characterization experiment setup

The true distance between the UWB nodes, $D_{true\ i,j}$ was estimated using a vision-based motion analysis system (Vicon Motion Systems Ltd, Oxford, UK), which for this study is regarded as 'gold-standard', as this system is capable of sub-centimetre level accuracy in estimating marker positions and distances (figure 2(a)). The UWB node position was defined as being located at the centre of the physical UWB antenna. As placing a physical reflective marker on the UWB antenna would very likely influence the ranging process, each UWB nodes were placed on a sensor-holding rig with 3 Vicon markers attached at some fixed distances away from the UWB antenna (figure 2(b)).

The reflective markers on the sensor-holding rig were labelled M1 to M3 (figure 2(b)). To estimate the position of the UWB node with respect to the rig an initial rig calibration procedure was performed, where the fixed relation between the UWB node antenna and the rig markers was derived. This was achieved through a static measurement of the rig markers with the Vicon system, with an additional temporary marker placed on the UWB antenna. This rig calibration measurement was then used to estimate the position of the UWB node during the experiment by utilizing the derived relation between the rig frame and sensor frame. Also, the UMIMU orientations were derived from the rig orientation.

2.4. Error characterization pipeline

The error characterization process involved multiple steps that were clustered into four phases: the preparation phase, the data collection phase, the data processing phase, and the error estimation phase (figure 3). The preparation phase involved setting up both the Vicon measurement system and the UWB nodes. This phase comprised the calibration of the Vicon system, followed by the UWB node antenna delay calibration and the rig calibration procedure as explained in section 2.3. The data collection phase involved the collection and storage of all the data from all 3 (or 2) UWB nodes and the Vicon system in all the experiments. The data processing phase consisted of estimating true distances from Vicon, processing measurements of the UMIMU sensors, synchronizing both the UMIMU and Vicon measurement systems, and preparing them for error computation. First, the true distances between the sensor nodes $D_{true\ i,j}$, were computed using the Euclidean distance method based on the marker positions measured by the Vicon system. Additionally, node accelerations, a_i^{vicon} were obtained by double differentiation of these positions. The accelerations from the MIMU sensors of the UMIMU sensor system, a_i^{uwb} were interpolated if there are any missing samples, and distances measured by the UWB nodes, $D_{uwb\ i,j}$ were parsed into readable arrays. Synchronization of the UMIMU and Vicon systems was then

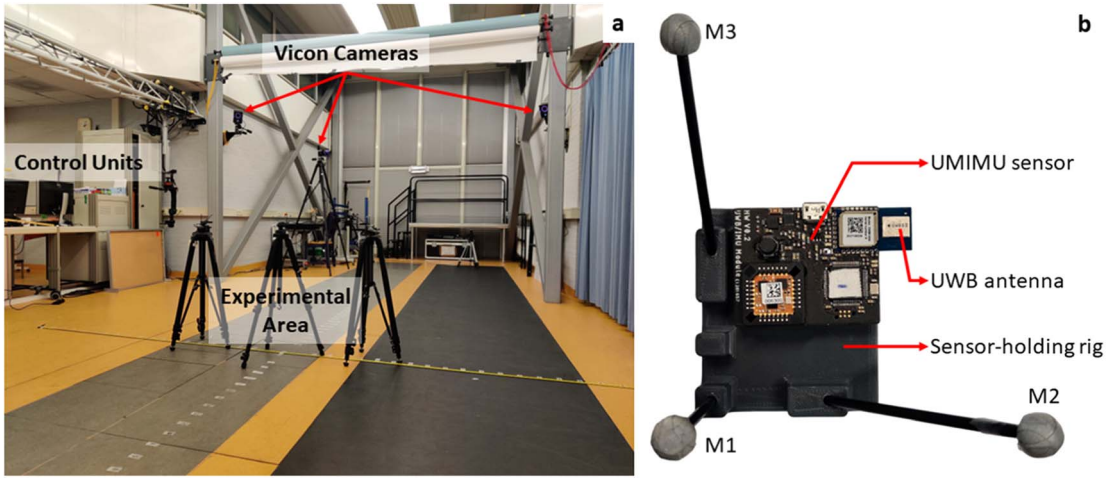

Figure 2. (a) Vicon optical motion tracking and analysis system; (b) Rig with the UMIMU sensor and the Vicon optical markers M1 to M3 on sticks at some distances of the UWB antenna.

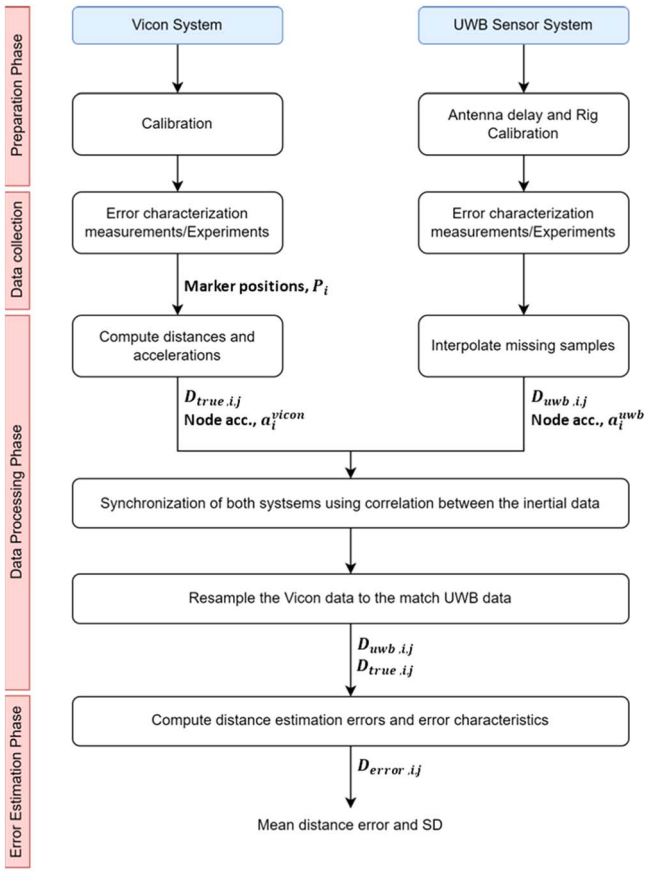

Figure 3. Illustration of the UWB error characterization pipeline.

achieved through cross-correlation of acceleration magnitudes derived from both systems, sampled at 100 samples per second (i.e., the norm of a_i^{vicon} and a_i^{uwb}). Subsequently after the synchronization between both the systems, the Vicon data was resampled to match the UWB update rates and instances using spline interpolation. Finally, for the error estimation phase, the errors in the distance estimates $D_{error\ i,j}$ were estimated by applying equation (1) for the resampled and synchronized distances from the UWB, $D_{uwb\ i,j}$ and the distances from Vicon measurement system, $D_{true\ i,j}$.

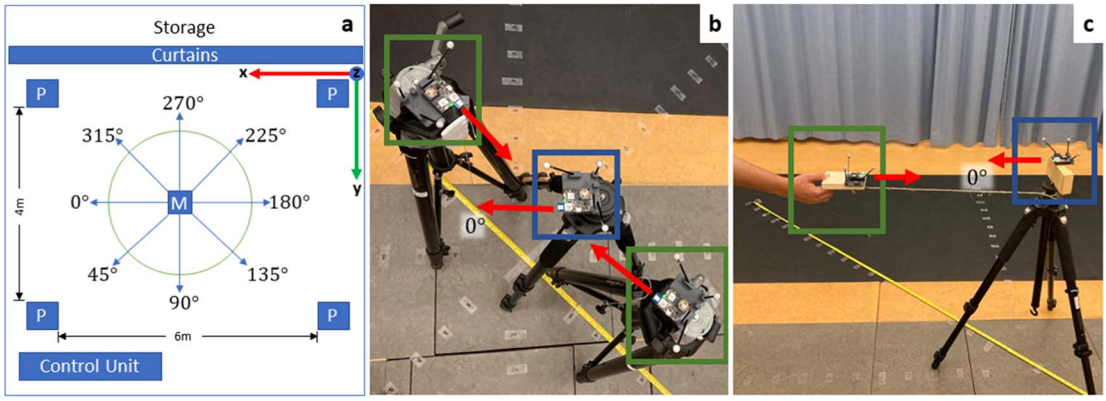

Figure 4. Overview of the LOS measurement scenario. (a) Schematic map of the room (not to scale), where P are metallic poles, and M is the position of the central node. The eight blue arrows indicate the eight different directions in which the two free nodes were moved. (b) Top view of the LOS static measurement with one central node (blue square) and two free nodes (green squares). The free node in the top left and bottom left is positioned in ranging headings 315° and 135°, respectively. (c) Overview of LOS dynamic measurement with central node (blue square) and one handheld free node on a wooden block (green square), at a fixed radius from the central node. (Red arrows in the figure indicate the antenna heading).

2.5. Experimental scenarios

The experimental scenarios were designed to consider the relevant situation of the 3D AHM. For both the LOS and NLOS conditions several scenarios were tested. This includes examining the effects of relative sensor position and relative sensor orientations in LOS conditions relevant to 3D AHM. Followed by the examination of the effects of NLOS caused by a subject's thorax and simulated human body segments, specifically PVC pipes filled with water with varying diameters as physical models of human limbs.

2.5.1. LOS in a static measurement scenario (Scenario 1)

In the static LOS measurement scenario, inter-UWB distances were measured with the sensor nodes positioned in multiple fixed positions and orientations, maximally securing LOS situations at all times. The objective of these measurements was to study the effect of antenna orientation and inter-node distances on their distance estimation accuracy. The experimental scenario comprised a 'central node', CN positioned on a tripod in a central location M and two 'free nodes' FN1 and FN2 mounted on tripods. The UWB nodes were always positioned in the same horizontal plane (xy-plane) of 0.84 m above the floor more or less in the center of a relatively large movement lab space (figure 4(a)). The central node was kept in the same position and orientation during the complete session, while the tripods of the two free nodes were moved to different positions for each measurement. A nomenclature was defined to describe the positions of the UWB nodes in the lab space and the horizontal direction of the two nodes with respect to each other. The 'ranging heading' was defined as the angle between the central node and one of the free nodes, with the global *x*-axis of the Vicon system reference frame chosen as a heading of 0°. The 'antenna heading' was defined as the direction in which the antenna of a node is facing using the same angles as used in the ranging heading. An example of the central node with an antenna heading of 0°, and two free nodes at ranging heading 315° and 135° with respect to the central node is depicted in figure 4(b).

In four different LOS protocols, distance estimates were collected in different combinations of free node distance to M, ranging heading, central node heading, and with free nodes elevated. In LOS-Protocol 1, the central and free nodes were placed at a height of 0.83 m above the floor. The free nodes were positioned on opposite sides of the central node and the distance estimates between the central node and the two free nodes were recorded for 30 seconds in each position. For each ranging heading the distance from the central node was increased in steps of 0.1 m after every 30 s of measurement, starting from a distance of 0.2 m up to a distance of 2 m. These measurements were repeated in all the 8 different ranging headings (figure 4(a)).

In LOS-Protocol 2, the same procedure as LOS-Protocol 1 was repeated for the ranging headings 90° and 270°, while keeping the antenna headings of the free nodes also at 0° (in the same antenna heading as the central node). This ensured all antennas of the ranging UWB nodes were parallel to each other. In LOS-Protocol 3, the same LOS-Protocol 1 was repeated, but with the antenna heading of the central node inverted, i.e., having an antenna heading the ranging direction of 180°. Also, this measurement was only performed with the free nodes for the four ranging headings of 0°, 135°, 180° and 315° respectively. In LOS-Protocol 4, LOS-Protocol 1 was repeated, but with the antenna heading of the free nodes turned upwards and the heights of the free nodes now being increased to 125.5 cm above the floor. The central node stayed at a height of 0.83 m and this

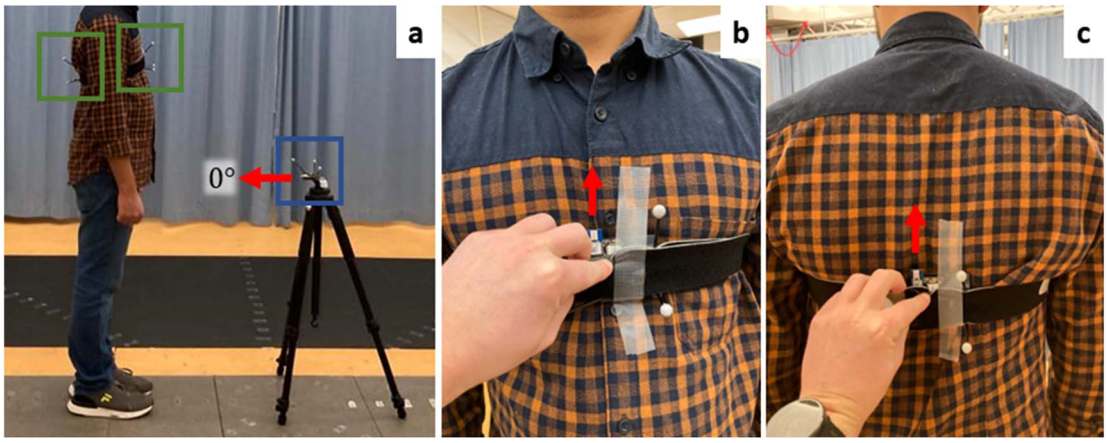

Figure 5. (a) Overview of the measurement setup with central node mounted on a tripod (blue square), and two nodes mounted on-body (green square), where human body acts as an NLOS obstacle between the DN and VN, as well as DN and CN. The red arrows indicate the antenna headings of the tripod node and respectively (b) the dorsal and (c) frontal body-worn nodes in more detail.

setting creates a perpendicular antenna heading between the ranging nodes. This LOS-Protocol 4 was performed for the ranging headings of 0°, 135°, 180° and 315° respectively.

2.5.2. LOS in a dynamic measurement scenario (Scenario 2)

In the dynamic experiment scenario of the LOS situation (LOS-Protocol 5), the UWB distance measures were acquired during a continuous change in position of the free node, with the central node remaining at its fixed position in location M at all times as seen in the static protocols. The moving free node was placed on a wooden block that was kept at a fixed distance from the central node by keeping a rope attached to the central tripod fully stretched (figure 4(c)). The wooden block was handheld by the researcher with a stretched arm to keep his body at a maximal distance to minimize the effects of body proximity to the ranging node (figure 4(c)). During the measurement, the researcher walked three circles around the static tripod, keeping the distance between the two ranging nodes fixed by keeping the rope fully stretched at all times. In total eight measurements with radius of 0.5 m, 1 m, 1.5 m, and 2 m were conducted for each of the two free nodes that were also used in the static trials.

2.5.3. Pilot experiment NLOS introduced by human body (Scenario 3)

In the NLOS situation introduced by the human body, static measurements were performed with a human torso as LOS blocking element. In this experiment, the central node was placed on a tripod at location M and the two free nodes were placed on the body of the human test subject (figure 5(a)). One of the free nodes was placed at the frontal side of the subject on the sternum (1.2 m above the floor) and was called the 'ventral node', VN (figure 5(b)). The second free node also named the 'dorsal node', DN was placed on the dorsal side of the subject at the same height as the ventral node (figure 5(c)). The subject was facing the central node at all times, thereby ensuring an NLOS situation between the dorsal node and ventral node, and also between the dorsal node and central node. Additionally, the distance between the ventral node and the central node was also measured. Though this specific distance measurement was in an LOS situation, it was still measured to study the effects on distance estimate due to close contact of the sensor with human body in LOS situations. The measurement protocol was similar to the one of LOS-Protocol 1, with the distance between the frontal node and central node increasing from 0.2 m by approximately 0.1 m every 30 s up to 2 m and in all the 8 ranging headings. The dorsal node remained at a fixed distance from the frontal node, while the distance with the central node was increased in steps of 0.1 m as moved along with the frontal node. Due to the limited field of view of the Vicon system, the true position of the dorsal node could not be estimated for distances larger than 1.3 m for the ranging headings 45°, 90°, 270° and 315°. Therefore, these were excluded from the analysis.

2.5.4. NLOS introduced by defined structures (Scenario 4)

For the experiments in scenario 4, the NLOS situations occurring when UWB nodes are used on a human body were emulated by using water-filled PVC pipes with varying diameters as a model for the human body. PVC was chosen to be the material of the container because of its relative permeance to electromagnetic fields causing minimal additional signal disturbance. Three PVC cylinders with diameters 4, 8, and 12.5 cm and a length of 80 cm were filled to the brim with water and subsequently sealed to ensure the safety of the measurement equipment and lab space.

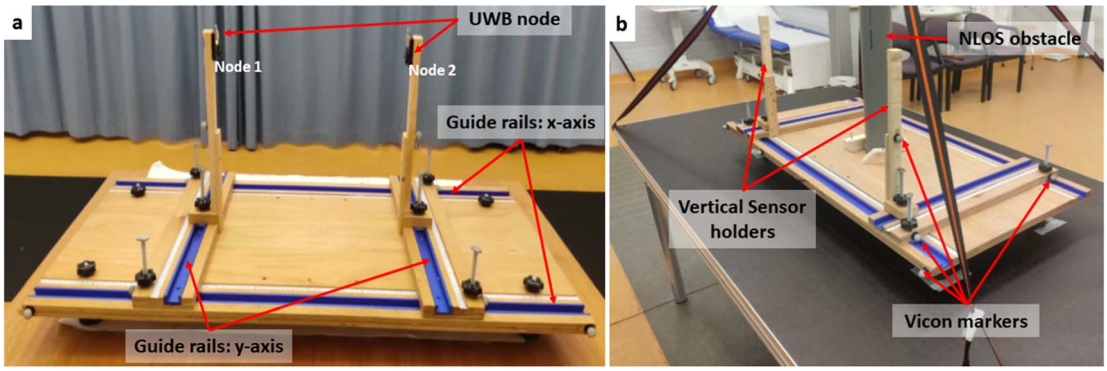

Figure 6. (a) Specialized platform for the NLOS experimental scenario; (b) A typical scenario during an experiment with the NLOS situation introduced with a PVC pipe in between ranging sensors on the setup.

A custom wooden measurement platform was constructed that holds the pipes in an upright orientation and allows accurate and quick (re)positioning of the ranging UWB nodes at any position (figure 6). The platform consists of a wooden base (1 m x 0.5 m plywood base) with guide rails on both the horizontal and vertical axis. It also consisted of two vertical sensor holders that can be moved in the horizontal plane along the guide rails (figure 6(a)). Rulers were attached along the guide rails to allow free and accurate placement of vertical sensor holders in a horizontal area of 0.8 m to 0.5 m. The platform was leveled through adjustable legs at its four corners and the UWB nodes were mounted at a height that was half of the length of the pipes. The center point of the platform was defined as the origin of the xy-reference frame. The PVC cylinder (simulated human body NLOS obstacle) was positioned at the center of the measurement platform in an upright position (figure 6(b)) with the two UWB nodes on each side of the obstacle. The true distances $D_{true\ i,j}$ between the UWB nodes were derived from the measured position of Vicon markers placed on the sensor holders. The true position of the UWB node antennas on the vertical sensor holders was calibrated with respect to the markers on the base of the sticks by performing an extra Vicon measurement with an extra marker positioned on the UWB antennas.

Two NLOS protocols were performed. In NLOS-Protocol 1, the pipe was placed in the origin and two UWB nodes were placed on opposite sides of the pipe on the X-axis. The UWB node on the left side of the pipe 'node 1' (figure 6(a)) was kept fixed at a set distance x1 from the pipe (NLOS obstacle). The UWB node on the right side 'node 2' (figure 6(a)) was positioned along the *x*-axis in steps of 1 cm starting from the closest point on the surface of the pipe to 0.3 m away from the central pipe, indicated by x2. This was repeated for multiple fixed distances x1 in increments of 1 cm. For each combination of positions x1 and x2 data was recorded with both the UWB and Vicon sensor system simultaneously for 10 s after the researcher had moved away from the platform. Before performing the NLOS-Protocols, a baseline measurement was obtained by performing the same protocol without the NLOS obstacle (PVC pipe), to identify and eliminate the additional errors caused by the measurement setup.

In NLOS-Protocol 2, data was gathered in different situations of the pipe (partially) eclipsing the line-of-sight between the two sensors. The pipe was kept fixed in the origin and both the UWB nodes were kept fixed along the *x*-axis with the distance between the pipe and each UWB node same (i.e., $x1 = -x2$, where x1 and x2 are the positions of node1 and 2 in *x*-axis respectively). Both the UWB nodes were moved in parallel along the entire *y*-axis (so always $y1 = y2$) in step sizes of 1 cm and 0.5 cm depending on the diameter of the pipe. For the pipe with a diameter of 12.5 cm, the step interval was 1 cm, while for the pipes with diameters of 8 and 4 cm, the step sizes were 0.5 cm. This was repeated for five different fixed distances along the *x*-axis, where x1 being respectively 17 cm, 27 cm, 37 cm, 47 cm, and 57 cm.

2.6. Data analysis

The main error metrics used in this study are mean of the distance measurement errors, $D_{error\ i,j}$ and their standard deviations (SD) for a particular position and orientation used in the experimental scenarios. For all static experiments of LOS situations in Scenario 1 the mean of distance measurement errors along with their SD were computed for each ranging heading and distance from a set of around 500 distance measurements (30 s at approximately 20 samples per second) at their respective positions. For the dynamic LOS experiments of Scenario 2, the mean of the distance measurement errors for each orientation was computed from the three circular movements made. For scenario 3, the mean and SD of distance measurement errors between the central node and ventral node on the body were computed for each ranging heading and distance from a set of around 500 measurements (30 s at approximately 20 samples per second) at their respective positions. Also, the mean

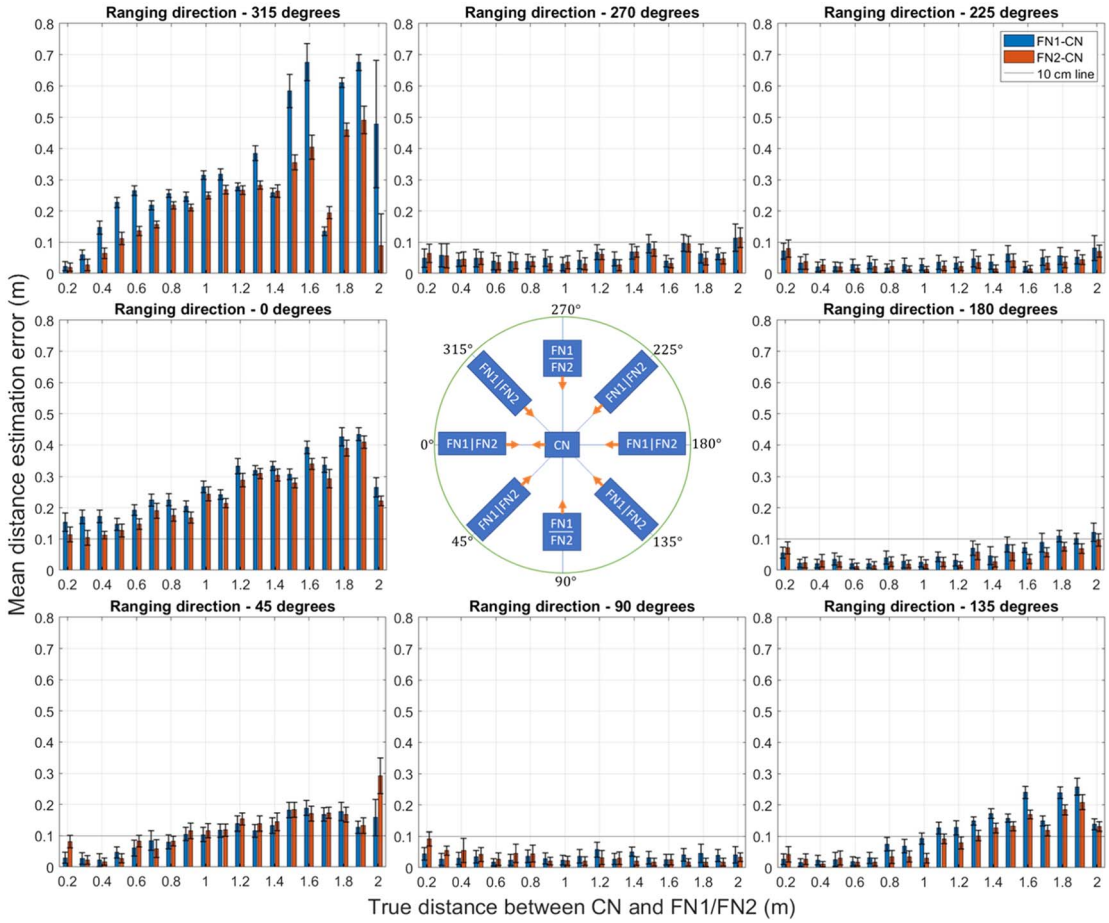

Figure 7. The mean distance measurement error and SD for the two ranging sensor pairs (FN1-CN and FN2-CN) in LOS-Protocol1 in all the eight antenna heading directions as well as multiple distances between 0.2 m to 2 m. The central figure is to represent the orientation of the sensors in this protocol, where the orange arrows indicate the antenna heading of the nodes.

and SD of distance measurement errors between both on-body sensors (ventral and dorsal node) were examined. For the NLOS experiments with the pipes of Scenario 4 again the mean distance errors along with their SD over each position with varying distances were computed.

3. Results

3.1. Ranging quality for LOS in a static measurement scenario

In all experiments of LOS-Protocol 1, the measurement error in the distance between the two free nodes and the central node, namely FN1-CN and FN2-CN were comparable and similar to each other in most measurement positions (figure 7). For the ranging headings 90°, 180°, 225° and 270°, all the mean distance measurement errors for FN1-CN and FN2-CN were below 10 cm for almost all measurement positions. Also, the mean distance error for each of these ranging headings was below 7 cm (figure 7). Conversely, for the ranging headings 0°, 45°, 135°, and 315°, the errors vary (mostly increase) with increasing distance between the ranging UWB nodes, also with mean distance errors higher than 10 cm for all ranging headings. The SD of the distance measurement was consistent and small (≈0.02 m) for almost all the ranging headings over all the varying distances. An exception was formed for some specific positions, where the SD was very high for ranging headings of 45° (for a distance of 2 m) and 315° (for distances of 1.5 m, 1.6 m and 2 m).

For LOS-Protocol 2, with the antenna headings in parallel orientation, the mean distance measurement errors for both the ranging headings were equal to or lower than 10 cm for most of the distances (figure 8). However, for a few measurements in the ranging heading 90° the errors were greater than 10 cm, specifically for distances above 1.3 m. The mean distance error for the two ranging headings 90° and 270° were 0.08 ± 0.03 m and 0.04 ± 0.02 m respectively. Similar to LOS-Protocol 1, the SD of the distance estimation was consistent and small (≈0.02 m) for both ranging headings over all the varying distances.

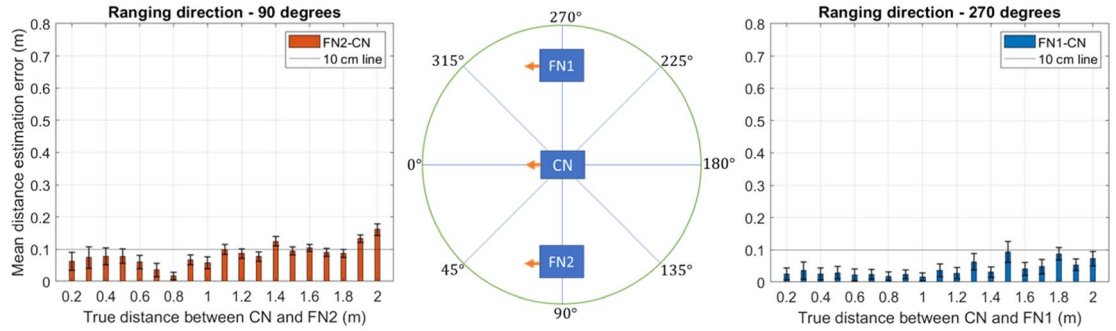

Figure 8. The mean distance measurement error and SD for the two ranging sensor pairs in the LOS scenario, with the antenna heading parallel to each other (LOS-Protocol2).

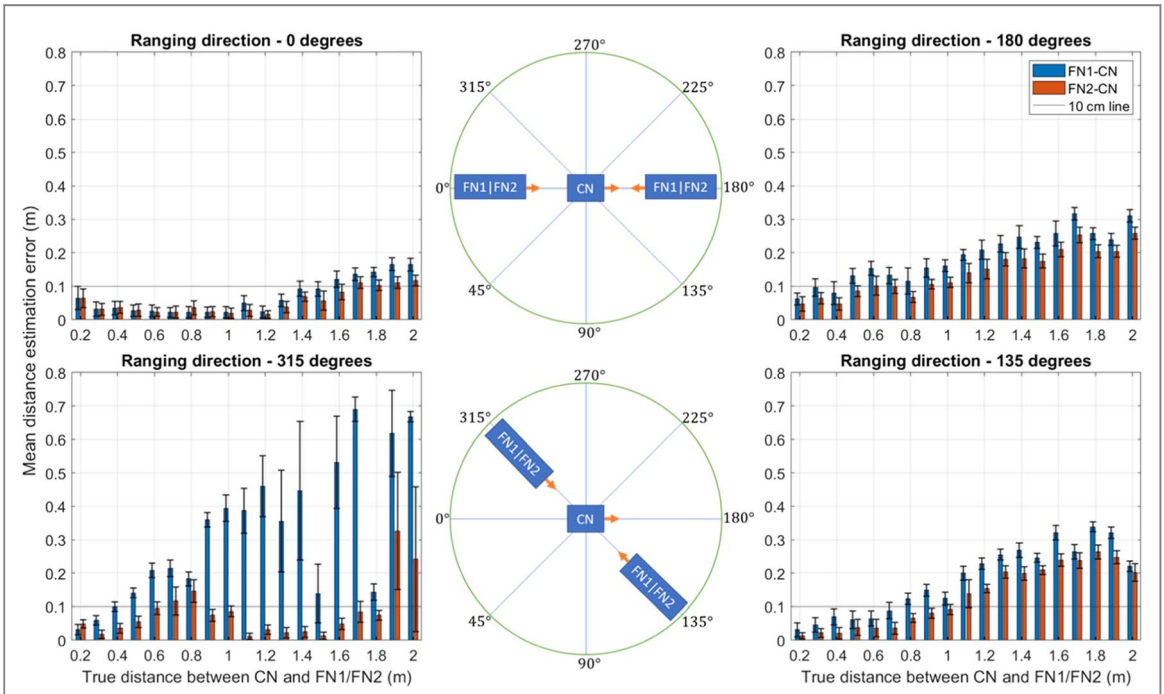

Figure 9. The mean distance measurement error and SD for the two ranging sensor pairs in LOS-Protocol 3 with the antenna heading direction of the central UWB node reversed.

Experimental results of LOS-Protocol 3, with the antenna heading of the central UWB node reversed (antenna heading: 180°) had comparable and similar distance measurement error for the node combination FN1-CN and FN2-CN, except for ranging heading 315° (figure 9). The mean distance measurement errors for the ranging heading 0° were lower than those of the LOS-Protocol 1, for both ranging node combinations. The errors in all measurements appear to increase with increasing distance. For the ranging heading 315°, the node combination of FN1-CN still exhibits high errors as the distance increases also with a high SD similar to LOS-Protocol 1. For the ranging heading of 90°, the node combination FN2-CN demonstrates errors mostly below 10 cm up to a distance of 1.8 m. The SD of the distance estimation was consistent and small (≈0.02 m) for almost all the ranging headings over all the varying distances, except for ranging heading 315° where SD was high with values up to 0.2 m.

For LOS-Protocol 4, the mean distance measurement errors were mostly below 10 cm and were also lower than the UWB-ranging situation in all the previous LOS protocols (figure 10). For directions 0° and 315°, there is a trend toward smaller errors as the distance between the nodes increases. In contrast, for 180°, the mean errors increase as the distance between the nodes increases. In this protocol, the SD of errors over all ranging headings and distances was consistent and small (≈0.02 m). The mean distance error from the two sensor combinations for all 4 ranging headings of LOS-Protocol 4 was always lower than 6 cm.

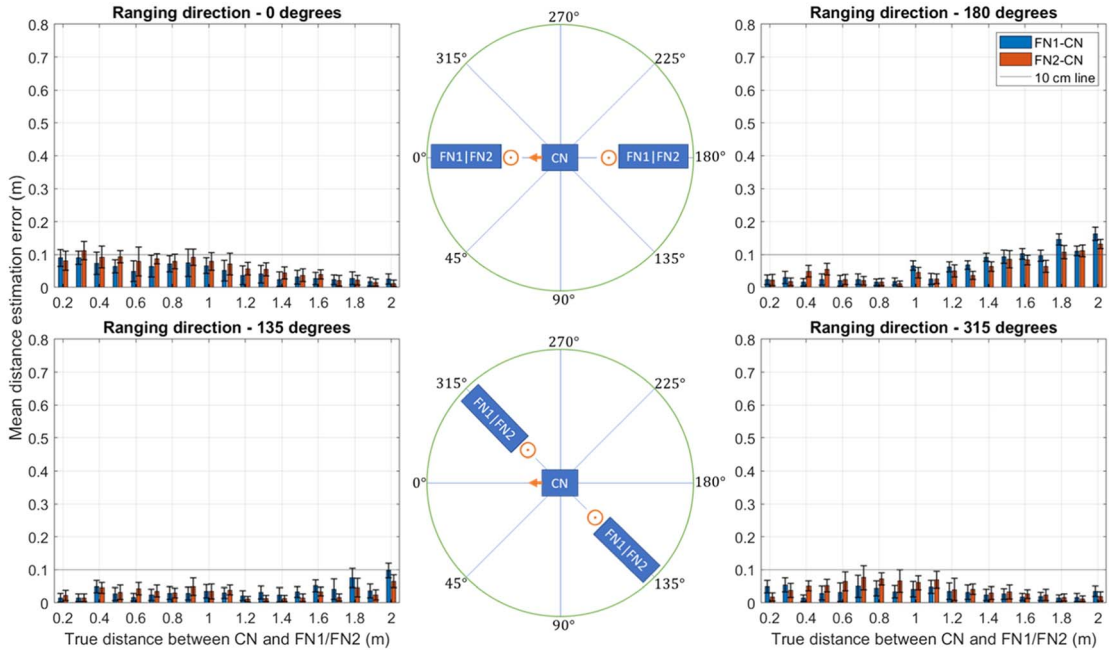

Figure 10. The mean distance measurement error and SD for the two ranging sensor pairs in LOS-Protocol 4 with increased height from the floor. The orange arrow and circles indicate the antenna headings, where the circle is to represent the antenna heading upwards.

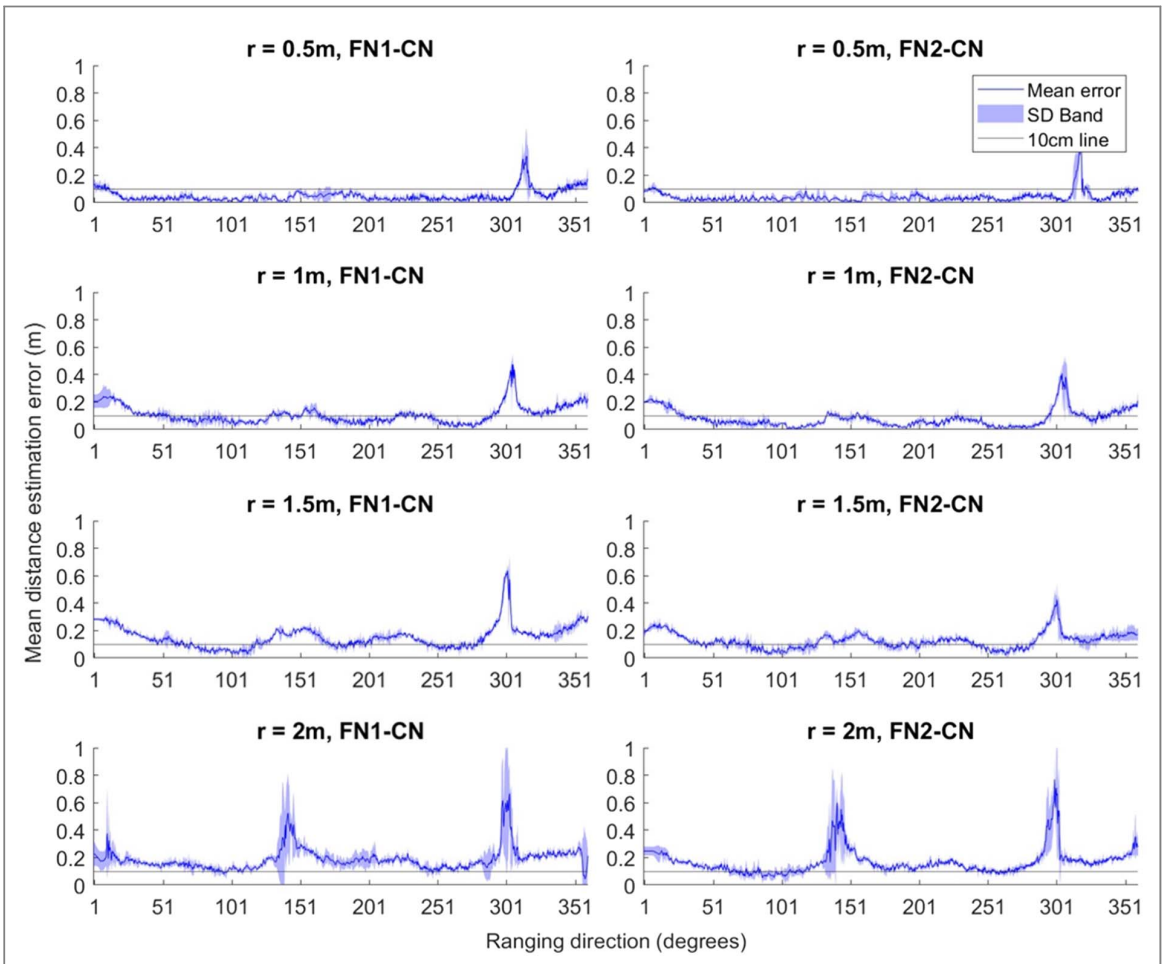

Figure 11. The mean distance measurement error and SD for the two ranging sensor pairs in the LOS dynamic scenario for all the ranging heading directions between 0° to 360°.

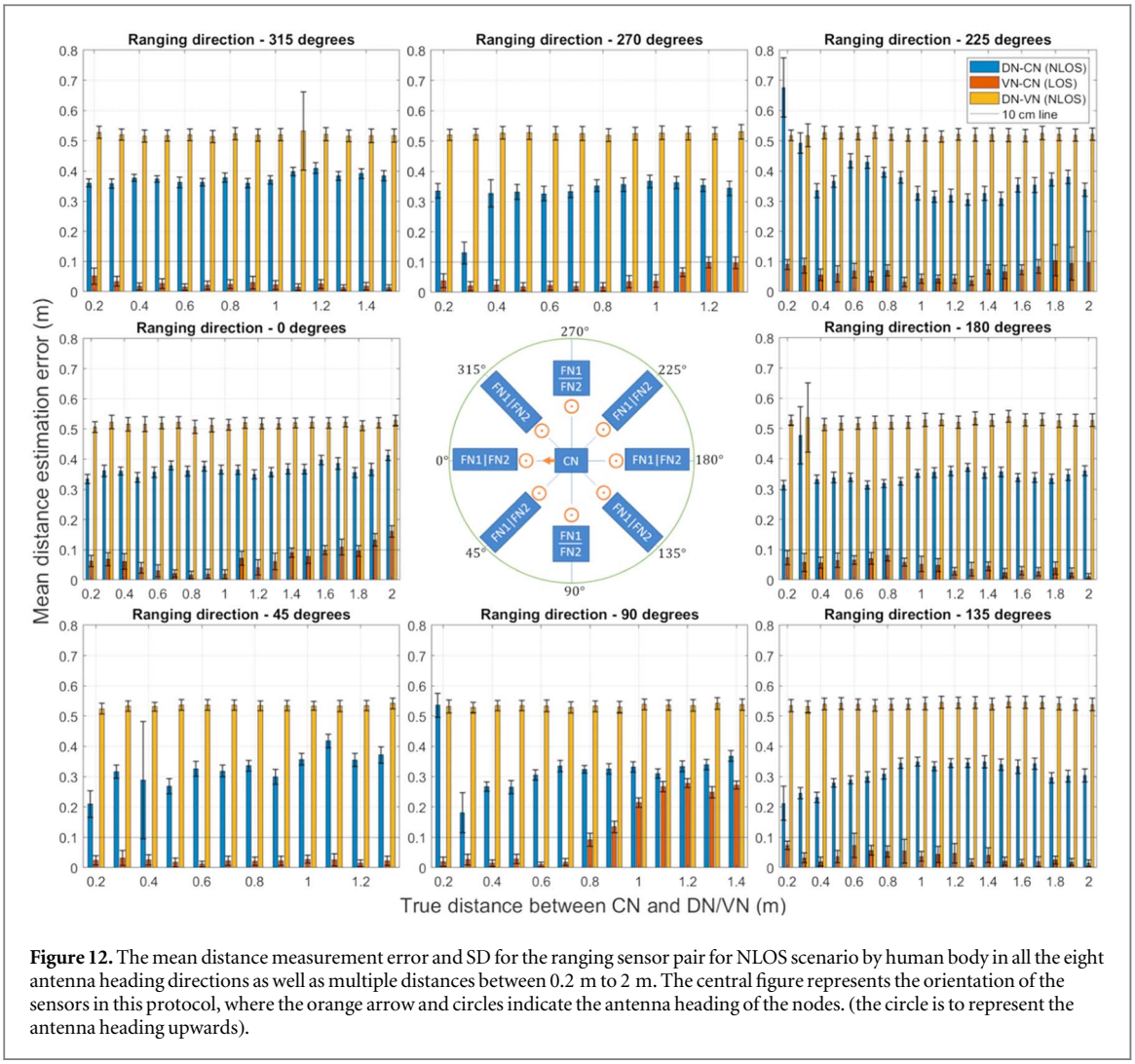

Figure 12. The mean distance measurement error and SD for the ranging sensor pair for NLOS scenario by human body in all the eight antenna heading directions as well as multiple distances between 0.2 m to 2 m. The central figure represents the orientation of the sensors in this protocol, where the orange arrow and circles indicate the antenna heading of the nodes. (the circle is to represent the antenna heading upwards).

3.2. Ranging quality for LOS in a dynamic measurement scenario

For all four radii in the dynamic LOS measurement scenario, an increased error (peaks) around the antenna heading direction of 315° was observed (figure 11). Also, for a higher radius of 1.5 m and 2 m, there is an increase in error around the antenna heading direction of 135°. The pattern of error is similar for all the radii, however, there is a slight increase in the overall error with an increase in distance of 1.5 m and above. The SD of errors was highly consistently below 3 cm, except for the errors around the ranging heading 315° and around 150° for radii higher than 1.5 m. Both the mean distance measurement errors and SD were similar to the static LOS protocols for all ranging headings.

3.3. Ranging quality for NLOS introduced by human body

The NLOS situations introduced by the human body have a significant effect on distance estimation with higher errors than the LOS situation (figure 12). The mean distance estimation errors between the UWB sensors on the back and sternum of the human subject (DN-VN) had a highly consistent error of around 0.53 m and a very low variability over varying ranging headings and distances (SD $<$ 0.01 m). For the sensor node combination between the dorsal and ventral node, DN-CN shows very consistent mean distance estimation errors of approximately 35 cm. The ranging between the ventral node, VN and the central node, CN was in LOS situations and the results indicate very similar distance estimation errors as seen in the LOS static scenario protocols. The mean distance estimation error from the three sensor combinations for all ranging headings was consistent with a small SD (figure 12).

3.4. Ranging quality for NLOS introduced by defined structures

The baseline distance measurements with the NLOS experimental setup show an effect of the setup on the distance measures between the UWB nodes (figure 13). After the correction of the distance measure by the

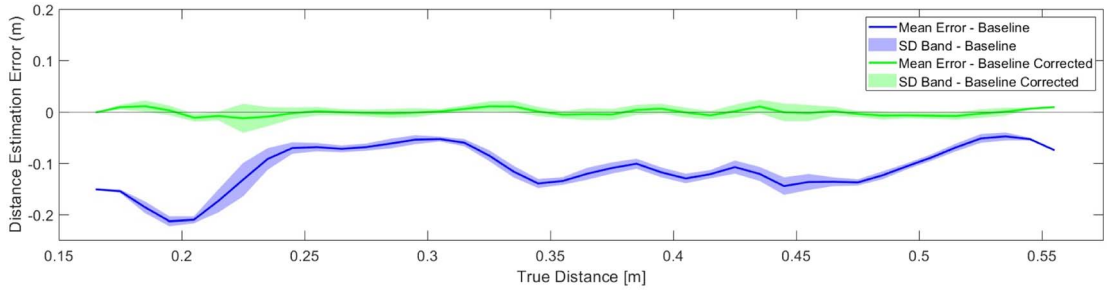

Figure 13. Baseline UWB ranging error as a function of the distance between sensors with no NLOS situation (blue) and baseline measurements after correction with the baseline error function (green).

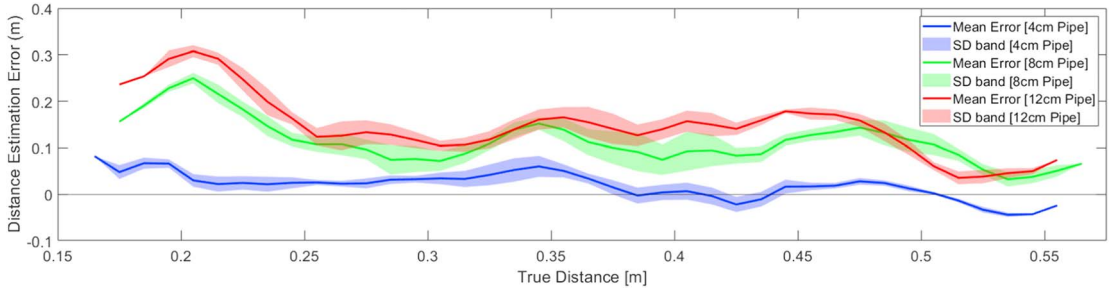

Figure 14. The mean distance measurement error (along with SD band) as a function of the distance between the ranging sensors from NLOS-Protocol 1, for the simulated NLOS situation with water-filled pipes of diameter 4 cm(blue), 8 cm(green) and 12.5 cm(red) respectively.

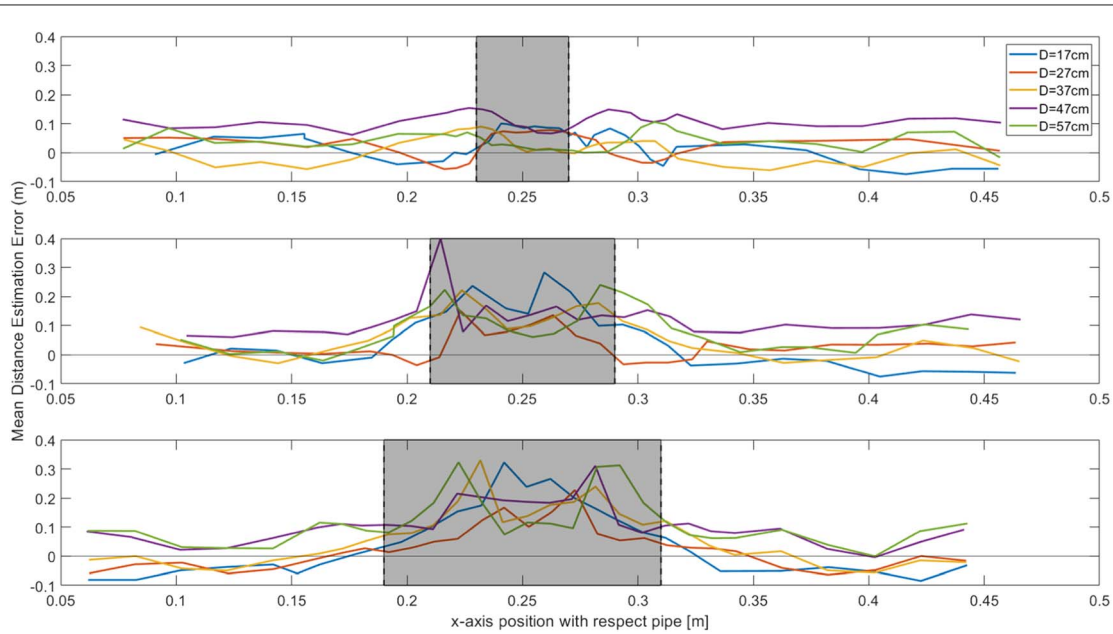

Figure 15. The mean distance measurement error as a function of position on the measurement table between the ranging sensors from NLOS-Protocol 2, for the simulated NLOS situation with a water-filled pipe diameter of 4 cm(top), 8 cm(middle) and 12.5 cm (bottom) respectively. The grey-shaded region indicates the position of the pipe.

estimated baseline correction values the UWB distance measures show a stable measurement with minimal errors around zero (figure 13).

Experimental results of NLOS-Protocol 1 showed mean distance errors that increased with the increasing diameter of the obstructing pipes (figure 14). The mean distance measurement errors of NLOS situation by 4 cm pipe was always within 10 cm for most of the distance points. For the NLOS caused by 8 cm and 12 cm pipes, the

errors increased with higher errors of 20 cm and above when UWB nodes were closer to the pipe. The SD for the baseline corrected mean distance errors are also provided in the graphs. The SD varied between 0.05 cm to 2.52 cm in NLOS with 4 cm pipe, while it was between 0.56 cm to 4.18 cm in NLOS with 8 cm pipe and the SD was between 0.06 cm to 3.30 cm in NLOS with 12 cm pipe.

For the NLOS-Protocol 2, the mean distance estimation errors were minimal for the NLOS situation with a 4 cm pipe, and only a slightly higher error was found close to the pipe (figure 15). For the other two NLOS obstacles, the position of the pipe is distinguishable from the ranging error as it increases when closer to the pipe. The errors always increased when closer to the pipe and dropped around the center of the pipe for all the NLOS situations of pipe with 8 cm and 12 cm.

4. Discussion

This study collected a comprehensive set of experimental data to examine the behavior of UWB node distance estimation errors under conditions relevant to the intended application scenario of 3D AHM. Different combinations of relevant ranging distances and sensor node orientations were examined in both LOS and NLOS situations. Firstly, the study provided a comprehensive distance estimation error analysis in static and dynamic LOS situations for the typical range of 3D AHM applications (0.2 m to 2 m). Secondly, a similar analysis was performed for the NLOS situation with two sensors mounted on opposite sides of the human thorax plus an external sensor at some distance. Following this, a more controlled NLOS situation, using water-filled PVC pipes simulating NLOS situations as they would be caused by human body segments, was studied. Inferences from the observed distance estimation error behaviour and its relevance to 3D AHM are further discussed in this section.

4.1. Distance measurement in LOS situations

4.1.1. Consistency and reliability of the measurements

The extensive study of the UWB distance measurement error in LOS situations was performed for two sensor node combinations (FN1-CN and FN2-CN). The resulting distance measurement errors from both sensor sets indicate that their performance was highly consistent, exhibiting very similar error values in almost all the experimental protocols. This indicates that the individual UWB nodes showed a consistent performance and provided confidence in the reliability of the measurement from the UWB sensor system being used. This also implies that sufficient care was taken to not influence the experiments by the presence of the human body (researcher) or other elements of the experimental set-up.

4.1.2. Effects of ranging headings

The results of LOS-Protocol 1 showed mean distance estimation errors below 6 cm for ranging headings 90°, 180°, 225° and 270°. They were slightly higher (between 8 to 12 cm) for ranging headings 45° and 135°, and very high (>20 cm) for ranging headings 0° and 315° (figure 7). In LOS-Protocol 3, the antenna heading of the central node was rotated to 180° and the mean distance errors of ranging headings 0° and 180° were reversed compared to the LOS-Protocol 1 (figure 9). This indicates that the increased error in the ranging heading of 0° is related to reduced signal strength between two ranging nodes that typically occurs when their antennas are facing each other [32].

4.1.3. Effects of antenna heading

For all the other ranging directions with higher errors, like the ranging heading 315°, 45 and 135°, the asymmetry in the distance error graphs in figure 7 suggests that this is not caused by ranging headings but by some unrelated cause. For example, the errors in the ranging direction 315° do not match the error from the ranging heading 45°. Also, unlike the case of headings 0° and 180°, in LOS-Protocol 3 the mean distance errors of ranging heading 315° remained similar to the previous condition but were not reversed, thus confirming that these errors were not an effect of ranging heading.

From the results of LOS-Protocols 1, 2 and 4, there is an effect of antenna heading found. In the LOS-Protocol 4, with the antenna headings of both nodes perpendicular to each other, the mean distance errors were always lower than 7 cm, suggesting it to be the best-relative antenna heading compared to others (figure 10). The LOS-Protocols 2 with the antenna headings parallel to each other, were the next antenna heading with lower errors than 8 cm. However, from the LOS-Protocol 1, it is clear that the antenna headings when facing each other have different errors over varying ranging headings and distances as described previously. This suggests that for these specific antenna heading configurations there is an error caused by a parameter that is not ranging heading or distance alone.

4.1.4. Errors due to additional interference

The observations from all these LOS static protocols as mentioned above clearly indicate the presence of an additional error, which is not relevant to the antenna heading or ranging heading. Also, there was an increase in the mean distance errors above 1.5 m in most of the ranging headings suggesting that within the range of 0.2 m to 1.5 m, errors are small and consistent. These inferences from the LOS static protocols thus suggest that the effect is a function of UWB node position in the room (3D space) as it is a combination of the ranging heading and distance from the central node with fixed position. This was again confirmed by the LOS dynamic experiments, where the distance errors become very high at around the ranging headings 135° and 315° as observed in the LOS static protocols (figure 11). In the dynamic experiments, this position-bound error manifests itself as a transient error occurring each time when the moving node passes specific positions, formed by specific combinations of ranging headings and distances. Also, these transient errors were clearly identified by very high variance (higher SD) in the distance estimates, which was otherwise very low and stable (≈2 cm).

4.1.5. Residual systematic errors

When neglecting position-based disturbances, there are only systematic offset errors of around 6 cm. These systematic errors were very consistent and repeatable, as was indicated by the very small SD values of the distance estimates. This was also confirmed by Schmid *et al* [33], where the errors were highly consistent and systematic offset of around 7 cm. Another study by Jimenez *et al* [34] reported mean errors as small as 12 cm and an SD value of 13 cm for an indoor environment with ranging distances between 0 and 5 m. However, this study by Jimenez *et al* was performed in a very dynamic measurement environment with strongly varying LOS and NLOS situation combinations. Though there were other studies in the literature, comparison of the results of this study against other studies was difficult due to varying measurement conditions. Most studies focus on ranges higher than 1 m (up to 20 meters or more) [15, 27–29], while this study focuses on ranges relevant to 3D AHM application (up to 2 m) providing a unique knowledge that has not been studied before.

4.2. Distance measurement in NLOS situations by human body

4.2.1. Experimental setup considerations

The UWB distance measurement errors in NLOS situations were studied through a pilot experiment with a (blocking) human body and under more controlled conditions with artificial obstacles with properties close to human body segments (water-filled PVC pipes). All the experiments in NLOS situations used parallel and perpendicular antenna heading configurations, as these had shown the best results in LOS situations. Additional distance estimation errors were observed for the situation of ranging between nodes on the platform without a pipe present. It is assumed that these errors were caused by adverse effects of the complex mechanical platform. Under this assumption, an independent baseline measurement was performed and all data of the experiments in the NLOS situations were compensated by subtracting the baseline error. The fact that all compensation values for the same node distance were found to be very similar (SD $<$3 cm), regardless of the position of both nodes, suggests that the additional errors were a function of the distance between the nodes and not of the position of both nodes on the platform. All distance errors found after baseline compensation were consistently small ($<$1.3 cm) and similar to error magnitudes in the LOS experimental results (figure 13), indicating a valid compensation.

4.2.2. Effect of NLOS caused by human body

The pilot experiments in NLOS situation with sensor nodes on the human body showed consistent, stable, and systematic overestimation errors in the distances between the UWB nodes. Experimental results showed a constant mean distance estimation error of approximately 0.53 m between the dorsal node and the ventral node (DN-VN), for all the subject positions in the experimental region (figure 12). These distance error estimations were highly consistent, indicated by the very low SD ($<$1 cm for all measurements). The errors seen in the human body NLOS situation fit the model that assumes that the distance estimate reflects the shortest distance around the obstructing body segment [17] and also are similar in magnitude to errors reported in [35]. Similarly, there was a consistent distance estimation error between 31 cm to 38 cm for distance measures between the dorsal node and the central node (VN-CN). This consistent effect remained the same throughout multiple ranging orientations and varying distances, except for the ranging orientation 90°. This was possibly due to the closeness of the subject to the electronic control unit of the Vicon measurement system in this specific position. Considering the inference from previous experiments in LOS situation, this effect would be a transient effect around that specific position.

Besides the effect of NLOS by direct obstruction of the human body, the UWB node combination VN-CN provides insights into the effect of being in close contact with human body in LOS situations. The closeness to the human body did not appear to have an additional effect on the distance estimation, which was evident from

the errors between the ventral node and central node being similar to, and as small as, those in the LOS situations without body presence.

4.2.3. Effect of NLOS caused by simulated human body segment

Experiments with NLOS situations by defined obstacles (the PVC pipes) showed a consistent overestimation of the distances between UWB nodes, similar to what was observed in the NLOS experiments with the human body. The distance estimation errors were more prominent and larger in amplitude with increasing PVC pipe diameters (figure 14). This suggests a strong relationship between the geometry of the obstructing object and the observed ranging error. Specifically, the amplitude of the ranging error was shown to be strongly linked to the size of the object, with the errors of the pipe with a diameter of 0.04 m being minimal and close to those of a pure LOS situation while the errors are larger for increasing pipe diameter. The error pattern again matches the simple wrap-around model that assumes that the distance estimate reflects the shortest distance around the obstructing pipe [17]. Though the mean errors increased, the SD of the distance measures by the UWB remained lower than 3 cm and were similar to those in the LOS measurement situation, indicating a repeatable measurement.

4.2.4. Comparative Analysis with Existing Literature

Only a few studies on the NLOS effect through the human body were found [15, 22, 26–29]. All these studies with the human body between the UWB nodes were studying ranging performance at distances larger than 1 m. In [29], distance estimation error was reported at around 0.18 m and 0.15 m for a fixed distance of 4 m and 7 m respectively between the UWB nodes with a human obstacle in the middle. Though a direct comparison of estimation errors of our study against [29] is not possible because of a different estimation range, the errors lower than 0.15 m with NLOS obstacle farther from sensors resonate similarly with the inference that a higher distance from the obstacle will have lesser error than being close to the obstacle. Jie *et al* [15] and Qinglin *et al* [22] studied the NLOS effect by placing UWB nodes on humans. However, only measurements were performed between the UWB sensor on the human body and an external UWB anchor more than 1 m away. Therefore, comparing [15] in ranges at 1 m and above confirms our observations that the ranging errors were higher (around 30 cm) when in NLOS by complete obstruction through the human body and errors were lower than 10 cm for on-body UWB in LOS with an external node. In addition to studying errors in the ranges relevant to 3D AHM, this study provides a very unique knowledge on measurements between on-body sensors both with human body and defined emulated human body segments.

4.3. Suitability for application in 3D AHM

The incidental higher errors observed in the LOS situation measurement appeared to occur as a function of absolute position in the room, as explained by the experimental static data (section 4.1). As in typical 3D AHM applications subjects are moving through space these errors will mostly manifest as transient errors, which was confirmed in the dynamic experiment data (section 4.1). In situations when a subject does hold a sensor in these specific positions for an extended period, the sensor data becomes invalid. However, since this issue can always be detected through different means using the redundant data set, this is not expected to be a critical problem. When these errors manifest as transients multiple opportunities arise to mitigate these error components, e.g. in the data fusion process of MIMU and UWB measurements with the proposed UMIMU sensors. Additionally, the UWB distance measurement fails when the distance between the ranging nodes is below 15 cm. However, with the commonly used sensor node placement on the human body in clinical gait analysis/3D AHM, this situation rarely occurs and typically manifests as a transient in the human movement data, which may be mitigated with the data fusion process.

Despite the UWB nodes being calibrated before the measurements following the manufacturer's indications (antenna delay calibration), a systematic residual bias error of around 6 cm was found in all measurements. This error level is considerably larger than the level deemed required for successful application in 3D AHM. However, as for each UWB node combination a specific consistent error magnitude was found, and a further improvement of the estimation error level seems feasible. This suggests that an additional systematic mitigation process for these persistent bias errors is feasible and should be researched in future studies. The perpendicular and parallel antenna headings configurations showed the smallest distance estimation errors (as observed in the results of LOS-Protocols 2 and 4). In terms of angles between the antenna headings of ranging UWB nodes, the ranging headings angles of 90°, 180°, 225° and 270° consistently showed the smallest errors. This information can be used to optimize choices in sensor orientation and position in sensor mounting protocols in 3D AHM applications.

The findings of this study suggest that NLOS situations caused by simulated human body segments will always cause an overestimation of the node distance that seems related to the size of the simulated body segment

causing the NLOS condition. This suggests that human body segments with smaller diameters such as the forearm and shank will have a smaller influence on the distance estimation, while the trunk and thighs will cause more substantial distance measurement errors. In our experiments, the effect of occlusion appeared consistent and repeatable. Therefore, these errors could possibly be mitigated through additional smart and automated systematic mitigation techniques to facilitate an accurate and stable application in 3D AHM.

5. Conclusion

This article provides a comprehensive analysis of the distance estimation errors between UWB node pairs, specifically for situations relevant to 3D AHM applications that have not been studied previously. The error analysis was performed for node distances in a range typically expected in 3D AHM applications (0.2 m to 2 m). Also, the effect of different node orientations was studied. Both static and dynamic LOS situations were examined, along with NLOS situations with human body and water-filled PVC pipes as physical models of human body segments. In LOS configurations, this study found errors of the consistent magnitude of around 6 cm for specific combinations of the relative position of nodes, (simulated) body and node orientation. This suggests the need for additional systematic error mitigation methods for UWB sensors. Small, consistent effects on the estimation error were found as a function of the relative ranging heading of the node antennas, providing valuable information for future on-body sensor placement. In both LOS and NLOS situations, no significant effect was observed on the closeness of the UWB nodes to the (simulated) human body. Large errors around 40 cm were found as a function of only the absolute position in the room, probably caused by reflection interference. In typical applications of 3D AHM (in which all sensors move most of the time), these errors will appear as transient errors in the data. This provides opportunities for error mitigation and appropriate independent detection of the presence of these transient errors. In NLOS situations a typical, consistent overestimation of the distance between UWB nodes was found. The amplitude of the distance estimation error was found to be a function of the object size as well as a function of the relative position to the object and appeared additive in nature. These observations made on the consistent character of UWB ranging errors within distance range and conditions relevant to 3D AHM will help to develop mitigating strategies for these errors in actual UMIMU data fusion-based applications in human movement analysis.

Data availability statement

The data cannot be made publicly available upon publication because they contain commercially sensitive information. The data that support the findings of this study are available upon reasonable request from the authors.

Author contributions

Vinish Yogesh: Conceptualization, Methodology, Validation, Formal Analysis, Writing—Original draft preparation **Jan Willem A. Rook:** Methodology, Validation, Formal Analysis **Thomas Keizers:** Methodology, Validation, Formal Analysis **Carsten Voort:** Methodology **Jaap H. Buurke:** Supervision, Writing—Review and Editing **Peter H. Veltink:** Supervision, Writing—Review and Editing **Chris T. M. Baten:** Conceptualization, Supervision, Writing—Review and Editing, Project Administration, Funding Acquisition

Conflicts of interest

The authors declare no conflict of interest. The funders had no role in the design of the study; in the collection, analyses, or interpretation of data; in the writing of the manuscript; or in the decision to publish the results.

Funding

This research was funded by the European Fund for Regional Development (EFRO) under grant number PROJ-000965.

ORCID iDs

Vinish Yogesh https://orcid.org/0000-0003-4309-0467

Jan Willem A Rook https://orcid.org/0009-0004-1881-8932

References

[1] Feng D, Wang C, He C, Zhuang Y and Xia X G 2020 Kalman-filter-based integration of IMU and UWB for high-accuracy indoor positioning and navigation *IEEE Internet of Things Journal* **7** 3133–46
[2] Hashim H A, Eltoukhy A E E and Vamvoudakis K G 2024 UWB ranging and IMU data fusion: overview and nonlinear stochastic filter for inertial navigation *IEEE Trans. Intell. Transp. Syst.* **25** 359–69
[3] Chow J, Hol J and Luinge H 2018 Tightly-coupled joint user self-calibration of accelerometers, gyroscopes, and magnetometers *Drones* **2** 6
[4] Kaichi T, Maruyama T, Tada M and Saito H 2020 Resolving position ambiguity of IMU-Based human pose with a single RGB camera *Sensors (Basel)* **20** 5453
[5] Li X, Wang Y and Liu D 2018 Research on extended kalman filter and particle filter combinational algorithm in UWB and foot-mounted IMU fusion positioning *Mobile Information Systems* **2018** 1587253
[6] Yogesh V, Buurke J H, Veltink P H and Baten C T M 2023 Integrated UWB/MIMU sensor system for position estimation towards an accurate analysis of human movement: a technical review *Sensors* **23** 7277
[7] Naheem K and Kim M S 2024 A robust indoor pedestrian localization approach against human body shadowing for UWB-Enabled smartphones *IEEE Trans. Instrum. Meas.* **73** 1–13
[8] Yavuzer G, Oken O, Elhan A and Stam H J 2008 Repeatability of lower limb three-dimensional kinematics in patients with stroke *Gait & Posture* **27** 31–5
[9] Carse B, Meadows B, Bowers R and Rowe P 2013 Affordable clinical gait analysis: an assessment of the marker tracking accuracy of a new low-cost optical 3d motion analysis system *Physiotherapy* **99** 347–51
[10] Zihajehzadeh S, Yoon P K and Park E J 2015 A magnetometer-free indoor human localization based on loosely coupled IMU/UWB fusion *37th Annual International Conference of the IEEE Engineering in Medicine and Biology Society* 2015 *(Milan, Italy)* 3141–4
[11] Kok M, Hol J D and Schon T B 2015 Indoor positioning using ultrawideband and inertial measurements *IEEE Trans. Veh. Technol.* **64** 1293–303
[12] Feng D, Peng J, Zhuang Y, Guo C, Zhang T, Chu Y, Zhou X and Xia X-G 2023 An adaptive IMU/UWB fusion method for NLOS indoor positioning and navigation *IEEE Internet of Things Journal* **10** 11414–28
[13] De Cock C, Tanghe E, Joseph W and Plets D 2023 Robust IMU-Based mitigation of human body shadowing in UWB indoor positioning *Sensors (Basel)* **23** 8289
[14] Naheem K and Kim M S 2022 A low-cost foot-placed UWB and IMU fusion-based indoor pedestrian tracking system for IoT applications *Sensors* **22** 8160
[15] Jie H, Yishuang G and Pahlavan K 2014 Toward accurate human tracking: modeling time-of-arrival for wireless wearable sensors in multipath environment *IEEE Sens. J.* **14** 3996–4006
[16] Haggenmiller A, Krogius M and Olson E 2019 Non-parametric error modeling for ultra-wideband localization networks *Proc. of the 2019 Int. Conf. on Robotics and Automation (ICRA), Montreal, Canada, 20/05/2019* 2568–74
[17] Chen J, Ye Y and Pahlavan K 2012 UWB characteristics of creeping wave for RF localization around the human body *Proc. of the 2012 IEEE 23rd Int. Symp. on Personal, Indoor and Mobile Radio Communications-(PIMRC), Sydney, NSW, Australia* 1290–4
[18] Wang F, Tang H and Chen J 2023 Survey on NLOS identification and error mitigation for UWB indoor positioning *Electronics* **12** 1678
[19] Nkrow R E, Silva B, Boshoff D, Hancke G, Gidlund M and Abu-Mahfouz A 2024 NLOS identification and mitigation for time-based indoor localization systems: survey and future research directions *ACM Comput. Surv.*
[20] Barbieri L, Brambilla M, Trabattoni A, Mervic S and Nicoli M 2021 UWB localization in a smart factory: augmentation methods and experimental assessment *IEEE Trans. Instrum. Meas.* **70** 1–18
[21] Nam S-C, Choi H-B and Ko Y-B 2021 On mitigation of ranging errors for through-the-body NLOS conditions using convolutional neural networks *Proc. of the 2021 23rd Int. Conf. on Advanced Communication Technology (ICACT), PyeongChang, Korea (South)*, 141–4
[22] Tian Q, Wang K I K and Salcic Z 2019 Human body shadowing effect on UWB-based ranging system for pedestrian tracking *IEEE Trans. Instrum. Meas.* **68** 4028–37
[23] Zhu J and Kia S S 2020 UWB ranging aided pedestrian geolocation with GPB-based Filtering for LoS and NLoS Measurement processing *IEEE/ION Position, Location and Navigation Symposium (PLANS), Portland, OR, USA* 781–7
[24] Zhu J N and Kia S S 2019 Bias compensation for UWB ranging for pedestrian geolocation applications *IEEE Sens. Lett.* **3** 7001704
[25] Sung S, Kim H and Jung J-I 2023 Accurate indoor positioning for UWB-Based personal devices using deep learning *IEEE Access* **11** 20095–113
[26] De Cock C, Tanghe E, Joseph W and Plets D 2023 Semi-unsupervised mitigation of human body shadowing for indoor UWB pedestrian tracking *Proc. of the 2023 13th Int. Conf. on Indoor Positioning and Indoor Navigation (IPIN), Nuremberg, Germany* 1–7
[27] Hamie J, Denis B, D'Errico R and Richard C 2013 On-body TOA-based ranging error model for motion capture applications within wearable UWB networks *Journal of Ambient Intelligence and Humanized Computing* **6** 603–12
[28] Smaoui N, Gnawali O and Kim K 2020 Study and mitigation of platform related UWB ranging errors *Proc. of the Int. Conf. on Communication Systems & Networks (COMSNETS), Bengaluru, India* 346–53
[29] Kılıc Y, Ali A J, Meijerink A, Bentum M J and Scanlon W G 2012 The effect of human-body shadowing on indoor UWB TOA-based ranging systems *Proc. of the 9th Workshop on Positioning, Navigation and Communication, Dresden, Germany* 126–30
[30] Neirynck D, Luk E and McLaughlin M 2016 An alternative double-sided two-way ranging method *Proc. of the 2016 13th workshop on positioning, navigation and communications (WPNC), Bremen, Germany* 2016, 1–4
[31] Qorvo 2024 Antenna Delay Calibration of DW1000-Based Products and Systems (APS014 Application Note), Rev 1.8, Available online: https://qorvo.com/products/d/da008449 (accessed on June 25, 2023)
[32] Qorvo 2016 DWM1000 Data Sheet, Rev 1.8, 2016. Available online https://qorvo.com/products/p/DWM1000#documents (accessed on March 20, 2024)
[33] Schmid L, Salido-Monz´u D and Wieser A 2019 Accuracy assessment and learned error mitigation of UWB ToF ranging *2019 Int. Conf. on Indoor Positioning and Indoor Navigation (IPIN), Pisa, Italy* 1–8
[34] Jimenez A R and Seco F 2021 Improving the accuracy of decawave's UWB MDEK1001 location system by gaining access to multiple ranges *Sensors (Basel)* **21** 1787
[35] Otim T, Bahillo A, Diez L E, Lopez-Iturri P and Falcone F 2019 Impact of body wearable sensor positions on UWB ranging *IEEE Sens. J.* **19** 11449–57